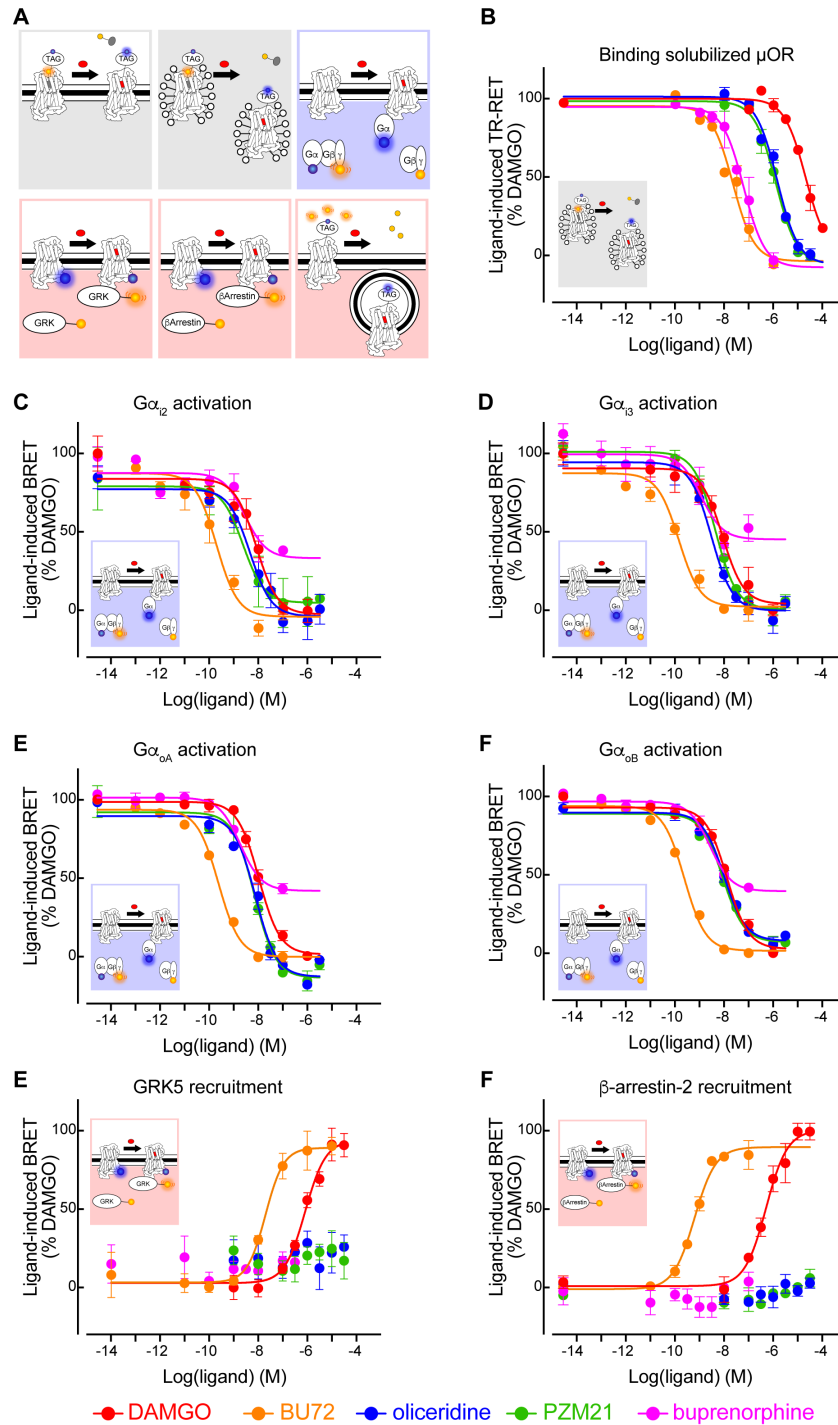


## Supplemental Information

<b>E<sub>max</sub> (% DAMGO)</b>	<b>DAMGO</b>	<b>BU72</b>	<b>Oliceridine</b>	<b>PZM21</b>	<b>Buprenorphine</b>
<b>Gαi1</b>	100	127 ± 17	94 ± 5	95 ± 6	63 ± 9
<b>Gαi2</b>	100	109 ± 8	98 ± 4	94 ± 5	66 ± 18
<b>Gαi3</b>	100	114 ± 14	94 ± 3	100 ± 5	83 ± 10
<b>GαoA</b>	100	120 ± 17	87 ± 5	90 ± 5	70 ± 5
<b>GαoB</b>	100	120 ± 14	91 ± 8	93 ± 9	67 ± 6
<b>GRK2</b>	100	98 ± 19	N.D.	N.D.	N.D.
<b>GRK5</b>	100	92 ± 8	N.D.	N.D.	N.D.
<b>β-arrestin-1</b>	100	98 ± 10	N.D.	N.D.	N.D.
<b>β-arrestin-2</b>	100	96 ± 12	N.D.	N.D.	N.D.
<b>Internalization</b>	100	96 ± 5	N.D.	N.D.	N.D.
<b>pEC<sub>50</sub></b>					
<b>Gαi1</b>	8.11 ± 0.13	9.76 ± 0.14	8.22 ± 0.09	8.22 ± 0.23	9.29 ± 0.77
<b>Gαi2</b>	8.33 ± 0.26	9.92 ± 0.24	8.59 ± 0.35	8.49 ± 0.33	8.90 ± 0.57
<b>Gαi3</b>	8.33 ± 0.22	9.99 ± 0.17	8.44 ± 0.05	8.51 ± 0.23	8.90 ± 0.51
<b>GαoA</b>	8.14 ± 0.20	9.55 ± 0.25	8.10 ± 0.09	8.12 ± 0.12	9.02 ± 0.72
<b>GαoB</b>	8.17 ± 0.24	10.10 ± 0.66	8.27 ± 0.32	8.25 ± 0.24	8.57 ± 0.21
<b>GRK2</b>	6.16 ± 0.22	8.19 ± 0.16	N.D.	N.D.	N.D.
<b>GRK5</b>	6.08 ± 0.13	7.65 ± 0.21	N.D.	N.D.	N.D.
<b>β-arrestin-1</b>	5.05 ± 0.17	8.40 ± 0.32	N.D.	N.D.	N.D.
<b>β-arrestin-2</b>	6.32 ± 0.12	9.00 ± 1.06	N.D.	N.D.	N.D.
<b>Internalization</b>	6.46 ± 0.17	8.96 ± 0.16	N.D.	N.D.	N.D.
<b>K<sub>i</sub> (nM)</b>					
<b>cells</b>	129 ± 50	0.7 ± 0.3	3.1 ± 2.5	6.7 ± 5.4	0.3 ± 0.2
<b>Solubilized μOR</b>	1255 ± 221	0.9 ± 0.7	66.0 ± 44.0	59.0 ± 33.0	2.3 ± 2.4

**Table 1. Potency, E<sub>max</sub> (relative to the maximal response of DAMGO) and affinity of the five ligands in assays. Related to Figures 1 and S1.**

Data presented as means ± S.D. of four to seven independent transfections performed in triplicates.



**Figure S1. Functional characterization of the five ligands. Related to Figure 1.**

(A) Schematic representation of the different BRET and TR-FRET assays used (donors are in blue and acceptors are in yellow). Dose-dependent response curves of the agonists in (B) competitive binding to solubilized  $\mu$ OR against fluorescent naltrexone, (C) activating  $G_{\alpha 2}$ , (D) activating  $G_{\alpha 13}$ , (E) activating  $G_{\alpha_{oA}}$ , (F) activating  $G_{\alpha_{oB}}$ , (G) inducing GRK5 recruitment, and (H) inducing  $\beta$ -arrestin-2 recruitment. Data shown are the means  $\pm$  S.D. of a representative experiment performed in triplicates normalized to the maximal response induced by DAMGO and fitted using an operational model of agonism.

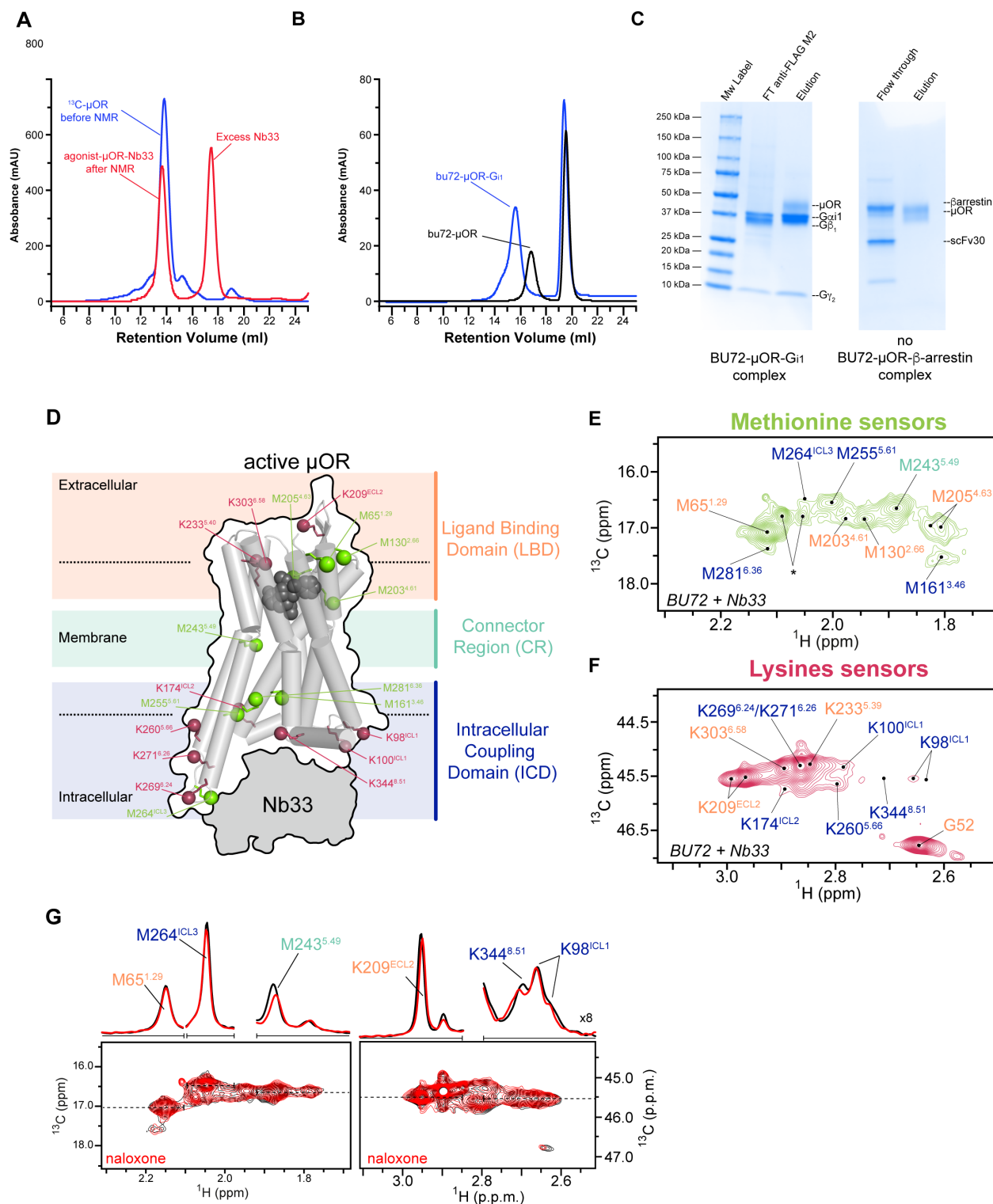


**Figure S2. Biophysical characterization of  $\mu\text{OR}$  complexes and development of NMR sensors. Related to Figure 2.**

(A) Typical size-exclusion chromatography (SEC) results showed the monodispersity of  $^{13}\text{C}$ -labelled  $\mu\text{OR}$  ( $^{13}\text{C}$ - $\mu\text{OR}$ ) before NMR (Blue) and the agonist- $\mu\text{OR}$ -Nb33 complex after NMR experiments (Red) using Superdex200 columns. (B) Typical SEC results showed the BU72- $\mu\text{OR}$ -Gi complex using Superose6

columns. **(C)** SDS-PAGE of BU72- $\mu$ OR-Gi1 complexes after anti-FLAG M2 resin pull-down confirmed the complex is made of  $\mu$ OR, G $\alpha$ i1, G $\beta$ 1, G $\gamma$ 2. In comparison, BU72- $\mu$ OR-arrestin complexes were not observed under the same condition. **(D)** Location of the NMR sensors in a cartoon representation of the BU72- $\mu$ OR-Nb33 ternary complex. NMR sensors,  $\epsilon$ -CH<sub>3</sub> of methionine (green) and  $\epsilon$ -NH<sub>2</sub> of lysine (raspberry), are shown in balls. **(E and F)** Extracted 2D HMQC spectra of the methionine and lysine sensors, as well as the backbone amine of the N-terminal residue G52, in the BU72- $\mu$ OR-Nb33 ternary complex. Asterisk indicates the peak positions of residual resonances of the N-terminal methionine in a small amount of untruncated <sup>13</sup>C- $\mu$ OR. **(G)** Comparison of HMQC spectra of  $\mu$ OR in apo-state (black) and saturating concentration of naloxone (red). 1D slices of HMQC spectra in the <sup>1</sup>H dimension is shown on top of each spectra.



**Figure S3. Assignments of resonances from methyl methionines of  $\mu$ OR in *apo* state and in complex with BU72 and Nb33. Related to STAR Methods.**

(A) Snake plot of  $\mu$ OR sequence showing the FLAG and 6x Histidine tags (light gray), the protease cleavable motifs (black), the M72<sup>1.36</sup>T mutation site (green, squared), as well as the methionine (green), lysine (raspberry) and G52 amine (red, squared) sensors. Unassigned residues in the 2D HMQC spectra are shown in hexagonal. (B) Comparison of the HMQC spectra of <sup>13</sup>CH<sub>3</sub>- $\epsilon$ -methionine labeled wild-type  $\mu$ OR (blue) and  $\mu$ OR-M72T (black) in *apo* state. (C and D) Spectra of methionine mutants in *apo* state and in the BU72- $\mu$ OR-Nb33 ternary complex. The spectra of  $\mu$ OR-M72T (black) was used as reference to superimpose those of the other mutants (red) We highlighted the peak disappearance for each mutant. We generated and recorded the NMR spectra for 12 mutants of 13 endogenous methionines (labeled in A). Only M151I could not be recorded because of instability issues. The spectra of M90I and M99L were not assigned under the conditions used.

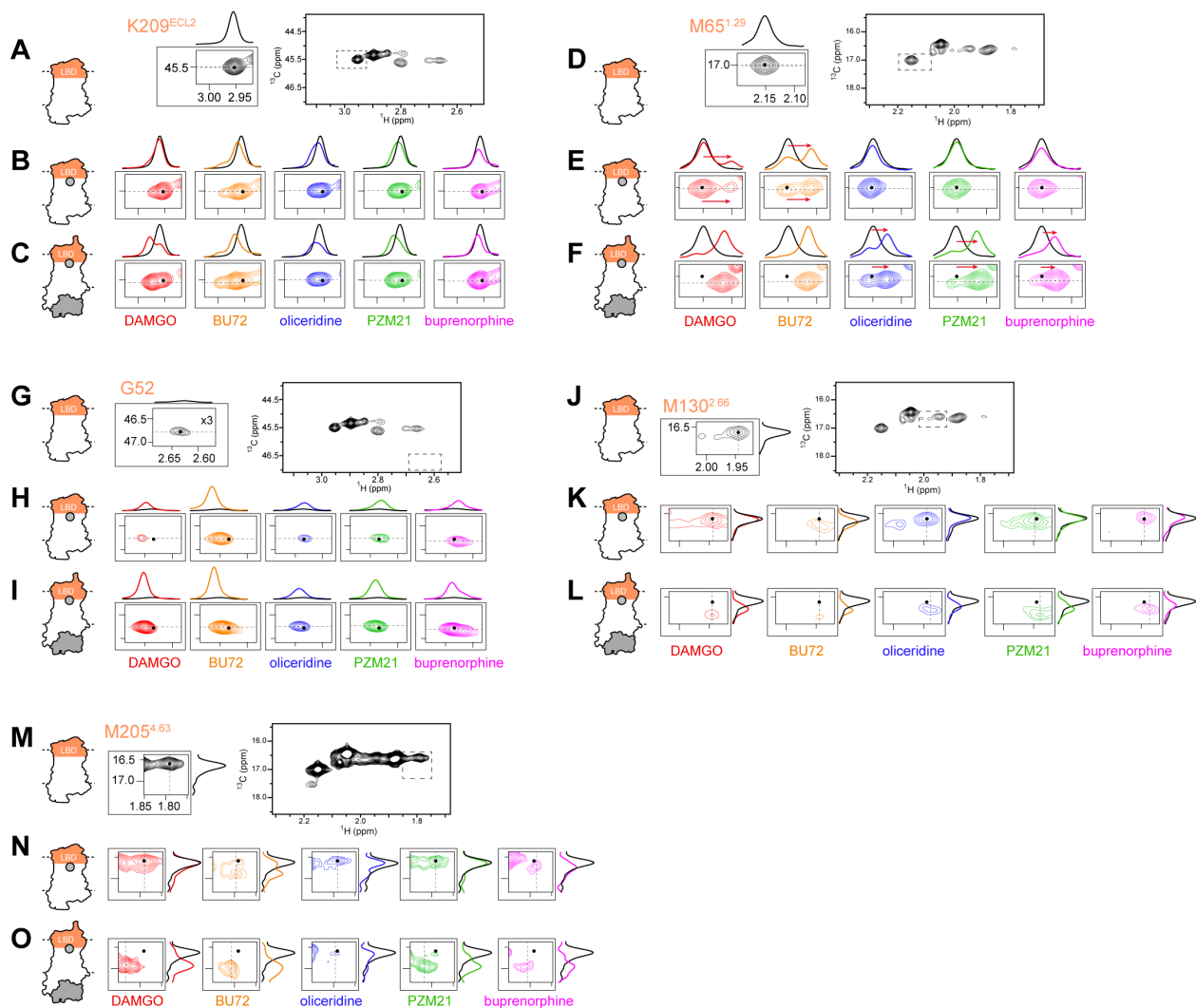


**Figure S4. NMR spectral changes in the ligand-binding domain upon binding with each agonist and Nb33 at saturating concentrations. Related to Figure 3.**

Extracted HMQC spectra of the sensors (A–C) K209<sup>ECL2</sup>, (D–F) M65<sup>1.29</sup>, (G–I) G52 amine at the truncated N-terminus), (J–L) M130<sup>2.66</sup>, and (M–O) M205<sup>4.63</sup> are compared with *apo*  $\mu$ OR (black) (top panel), either bound to agonist (middle panel) or to agonist and Nb33 (bottom panel). Dashed black lines indicate the position of the cross-sections shown on top or on the right of the spectra.

The K209<sup>ECL2</sup> (A–B) and M130<sup>2.66</sup> (J–K) probes only sensed slight effects of ligands alone with a decrease of signals intensity and a downfield shift of the chemical shift in the <sup>1</sup>H dimension and <sup>13</sup>C dimension. By opposition, for those two sites, Nb33 binding to the agonist-bound receptor induced important changes both in intensity and <sup>1</sup>H chemical shift for all the tested ligands (C and L). The N-terminus G52 probe sensed the binding of all ligands with a peak appearance (2.64 ppm and 46.75 ppm in <sup>1</sup>H and <sup>13</sup>C dimension) further increased in intensity upon Nb33 binding (G–I). These results suggest that the N-terminus of the *apo* form of the receptor sample more conformations than bound states. Of note, Nb33 binding at the ICD further increased the G52 methyl peak, suggesting a further stabilization of the N-terminus. Interestingly, the M65<sup>1.29</sup> probe revealed a ligand-specific regulation in which only BU72 and DAMGO by themselves were able to modify the chemical shift obtained in ligand free preparation (D–F). In particular, BU72 and DAMGO promoted the appearance of a new peak at 2.12 ppm in the <sup>1</sup>H dimension (E). In the presence of Nb33, the biased ligands were able to induce a similar effect than BU72 and DAMGO alone (F). However, the presence of the two peaks with different intensity suggest substantial slow conformational exchange

between different states. Of note the peak from the unliganded state (2.15 ppm) totally disappeared in the ternary complex samples for non-selective agonists (BU72, DAMGO). The NMR cross-peak of M205<sup>4,63</sup> in the HMQC spectra is highly dependent of the bound ligand. The distinct effects between agonists may be due their different chemotypes (**Figure 1A**). However, binding of ligands results in the appearance with two new close peaks at the downfield resonance in the <sup>13</sup>C dimension together with a highly broadening/splitting of the apo peak (BU72), in the increase and broadening towards downfield <sup>13</sup>C shift signal intensity (DAMGO), in the loss of signal intensity (e.g., oliceridine, buprenorphine) or no changes (e.g., PZM21) (**M**). As observed with M65<sup>1,29</sup>, binding of Nb33 at the ICD causes more drastic changes in the NMR resonance of M205<sup>4,63</sup>. Particularly for all agonists, we observe the appearance of multiple peaks, which shifts downfield from the apo-state peak for both <sup>1</sup>H and <sup>13</sup>C dimensions, recovering the new peak observed in the binary complex with BU72 (**O**). These observations suggest that the local conformation may become more dynamics and multiple conformations that exchange on the intermediate or slow NMR timescales.



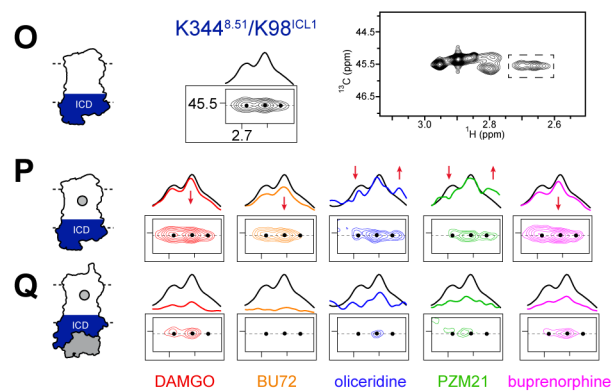
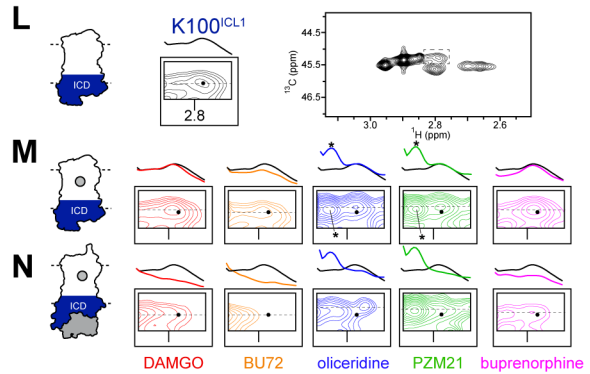
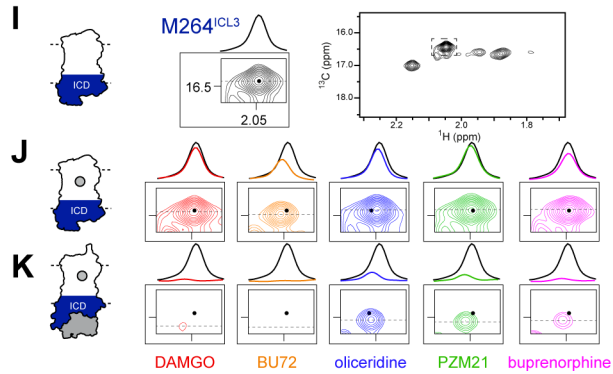
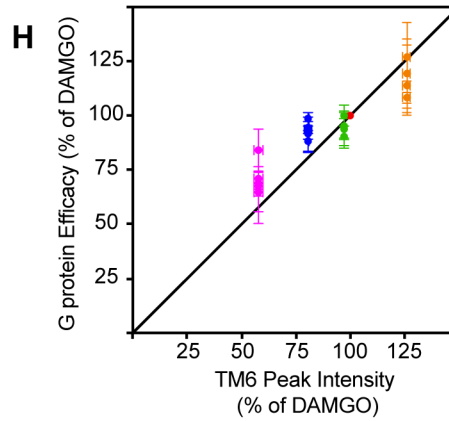
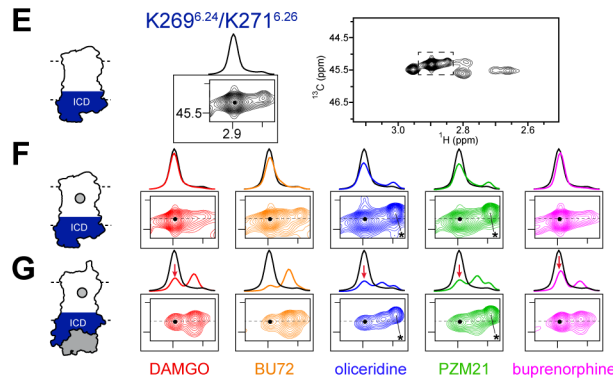
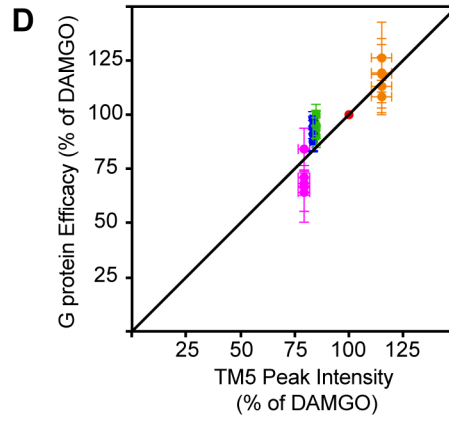
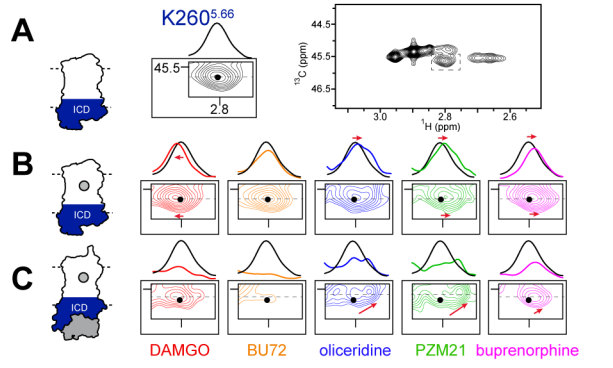


**Figure S5. NMR spectral changes on the intracellular coupling domain upon binding with each agonist and Nb33 at saturating concentrations. Related to Figure 5.**

Extracted HMQC spectra of the sensors (**A—C**) K260<sup>5.66</sup>, (**E—G**) K269<sup>6.24</sup>/K271<sup>6.26</sup>, (**I—K**) M264<sup>ICL3</sup>, (**L—N**) K100<sup>ICL1</sup> and (**O—Q**) K344<sup>8.51</sup>/K98<sup>ICL1</sup> are compared with *apo*  $\mu$ OR (black) (top panel), either bound to agonist (middle panel) or to agonist and Nb33 (bottom panel). Dashed black lines indicate the position of the cross-sections shown on top of the spectra. Black dots indicate the peak centers of *apo*  $\mu$ OR. Asterisks in (M) and (N) indicates signals from impurity most likely comes from the uncleaved N-terminus. Agonist efficacies for G proteins correlate with the changes in the peak intensities at (**D**) K260<sup>5.66</sup> and (**H**) K269<sup>6.24</sup>/K271<sup>6.26</sup> in the ternary agonist- $\mu$ OR-Nb33 complexes. DAMGO is used as reference (set at 100%). Verticals error bars indicate SEM for each of the five Gai/o proteins (Table S1). Horizontal error bars represent the uncertainty in volume determination due to random noise.

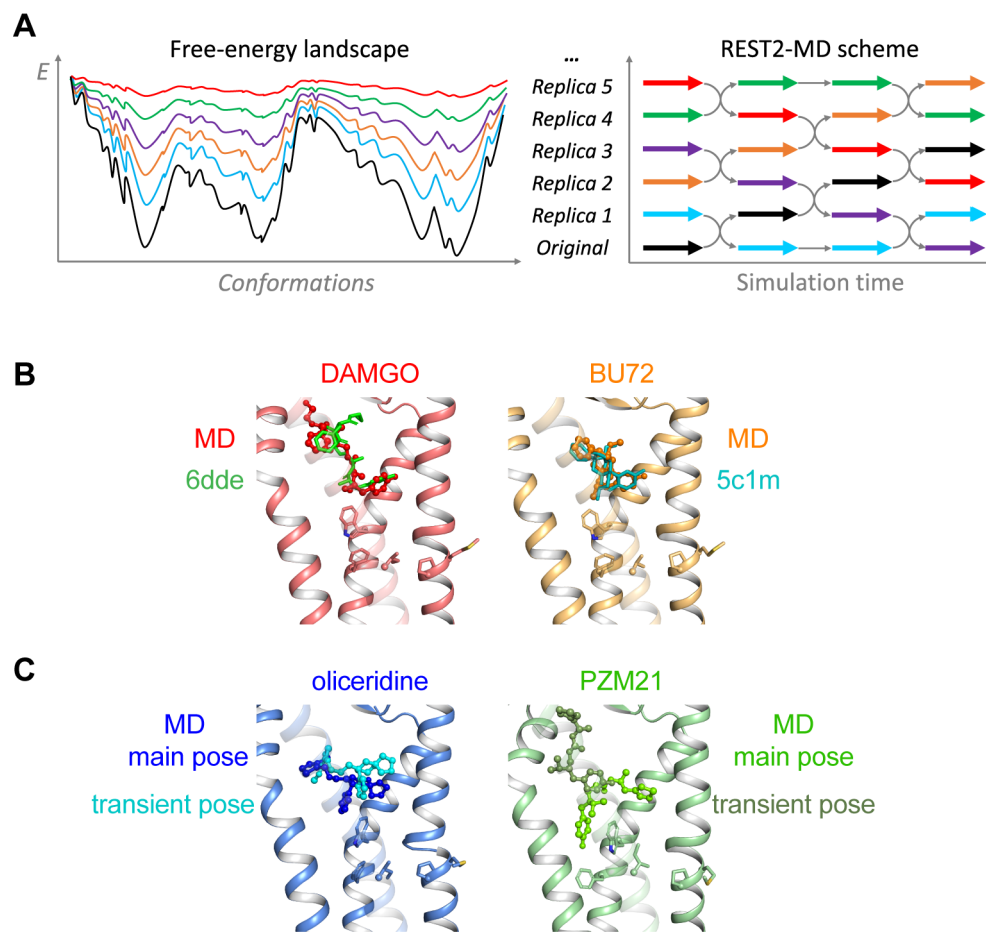


**Figure S6. REST2-MD simulation scheme and ligand binding poses captured by REST2-MD. Related to STAR Methods.**

(A) REST2-MD performs many replicas of the same simulation system simultaneously. The replicas have flatter free energy surfaces to ease barrier crossing. By frequently swapping the replicas during the MD, the simulations “travel” on different free energy surfaces and easily visit different conformational zones. (B) The binding poses of DAMGO and BU72 reproduced those in the experimental structures (PDBs 6DDE and 5C1M, respectively). (C) Transient binding poses of oliceridine and PZM21 compared with the main poses.

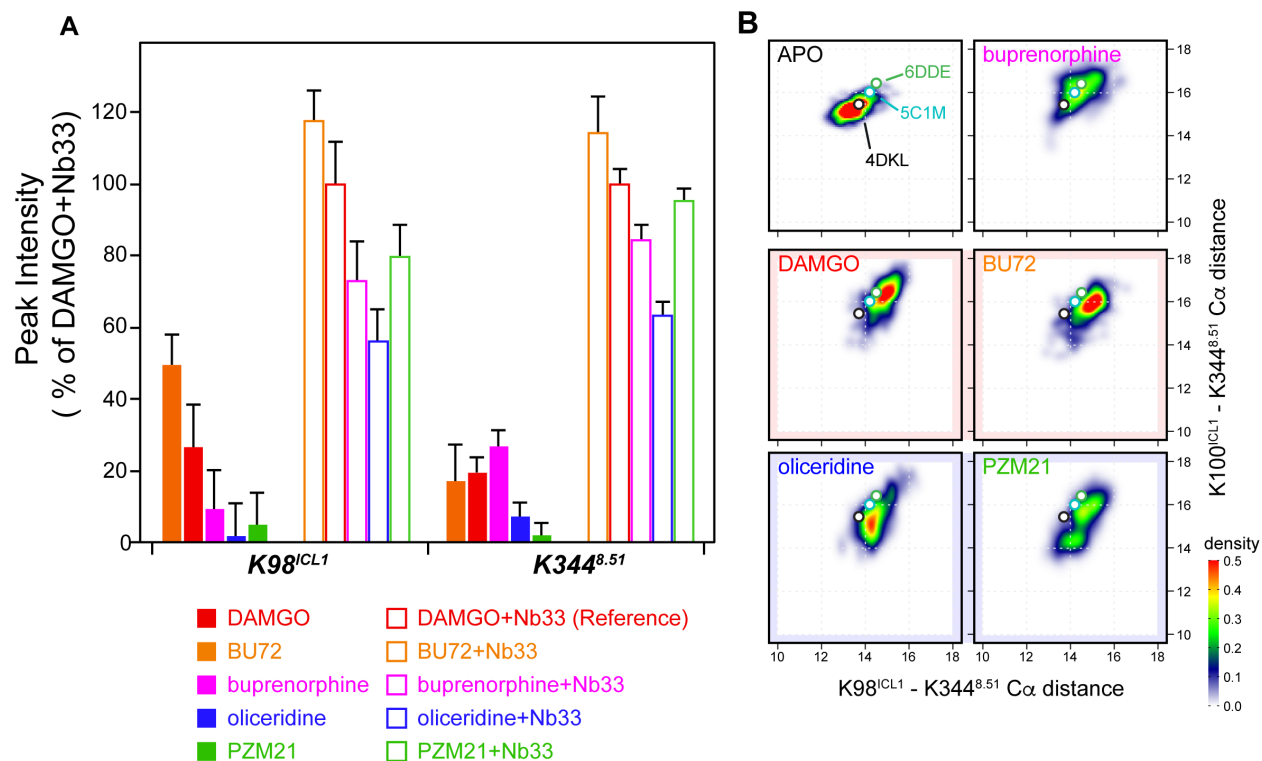


**Figure S7. Conformational changes of ICL1/H8 upon binding the agonists and Nb33. Related to Figure 5.**

(A) Peak intensities were normalized to the volume difference between the *apo* state and DAMGO- $\mu$ OR-Nb33 ternary complex as the 100%. Error bars represent the uncertainty in volume determination due to random noise. (B) Density maps of the  $C\alpha$  distances between  $K98^{ICL1}$ ,  $K100^{ICL1}$  and  $K344^{8.51}$  during REST2-MD of the agonist- $\mu$ OR-Nb33 ternary complexes, compared with the *apo* state and the values in experimental structures ((PDBs 4DKL, 6DDE and 5C1M).